JOURNAL OF CATALYSIS 103, 480–491 (1987)

Deoxygenation of Methanol with Carbon Monoxide over Fe/ZSM-5 Catalysts

INTRODUCTION

Deoxygenation is a process of interest in the upgrading of various feedstocks including liquids derived from biomass. Wood liquefaction techniques, especially by pyrolytic processes, yield highly oxygenated products. Two catalytic routes have been proposed for deoxygenation of pyrolytic oils (*1*), namely, hydrotreatment with H_2 or $CO + H_2$ over HDS-type catalysts, and dehydration or decarboxylation over zeolite-type acid catalysts. As pointed out by Overend (*2*) dehydration has a disadvantage in oxygen removal: starting with a material of high oxygen content (typically H/O/C ~ 1.5/0.4/1 in pyrolytic oils) the mixture of the products of pure dehydration has an overall H/C ratio much lower than in typical fuels (H/C = 1.9 in gasoline). In order to eliminate this major inconvenience, it is proposed in this work to add to the zeolite catalyst a water-gas shift (WGS) function. Over such a bifunctional catalyst it is proposed to feed an oxygenate compound in a stream of carbon monoxide. In such a process, oxygen will be eliminated as CO_2 rather than H_2O, and if the WGS active catalyst possesses some hydrogenation properties under the operating conditions, the molecular hydrogen generated by WGS may be reincorporated into the growing hydrocarbon chains.

The zeolite component selected is ZSM-5 due to its shape-selectivity properties for the formation of gasoline-range hydrocarbons and its resistance toward coke building. Indeed, studies have demonstrated the ability of ZSM-5 to convert a wide range of oxygenated products into gasoline-range hydrocarbons with a high selectivity (*3, 4*). Complex mixtures derived from biomass have also been reacted over ZSM-5 (*5–10*). For instance, a recent study (*10*) has shown that 10 to 15% of a pyrolytic oil produced by supercritical extraction of aspen poplar wood can be transformed into C_5 to C_{10} hydrocarbons without any preliminary fractionation of the oil.

Iron oxide has been chosen as the second component of this dual function catalyst since it is a conventional WGS catalyst compatible with the high temperature required for the conversion of the pyrolytic oil over ZSM-5 (*11*).

Methanol has been used as a probe reactant to test the performance of this dual function catalyst Fe_2O_3/ZSM-5.

An alternate route for the use of wood as source of chemicals or fuels is indirect liquefaction via gasification to synthesis gas followed by conversion to hydrocarbons over a Fischer–Tropsch (F–T) catalyst. Many studies have shown that direct conversion of synthesis gas to gasoline-range hydrocarbons can be performed over a combination of a F–T active metal, such as iron, with ZSM-5 (*12–16*). In this context, it was interesting to test our Fe/ZSM-5 catalysts for this reaction.

Another important aspect of this study is the development of a new method for the deposition of iron on ZSM-5. The use of metal carbonyls has been presented as an appropriate means to introduce iron into the porous structure of zeolites, especially faujasite-type molecular sieves in order to synthesize highly dispersed supported

0021-9517/87 $3.00

metal catalysts (*17*). Unfortunately, even the smaller carbonyl $Fe(CO)_5$ is too bulky (diameter ~7 Å) to enter the pore system of ZSM-5 (5.1 to 5.7 Å) (*18*). For this reason, we propose to employ ferrocene, which has smaller dimensions (4.4 × 3.3 Å) (*19*) than the pore diameter of ZSM-5. Moreover, this type of compound also offers the possibility of controlling the location of iron on the support. A bulky radical, like the dibenzoyl radical, can be added effectively as a substituent on the cyclopentadienyl rings. The large size of this new complex would prevent the diffusion of the organometallic compound into the pores, and consequently, it would allow fixing the iron on only the external surface of the ZSM-5 grains.

EXPERIMENTAL

Catalyst preparation. ZSM-5 samples were synthesized according to a method described as method B′ by Gabelica *et al.* (*20*). A gel formed by mixing Q-brand sodium silicate, aluminum sulfate, tetrapropylammonium bromide, sulfuric acid, and water is heated at 410 K in an 800-ml Teflon-lined autoclave for 6 to 7 days. The product is then filtered, thoroughly washed with deionized water, and calcined at 800 K to burn off the organic matter, yielding the Na^+ form Na-ZSM-5. The conversion to the active protonated form, H-ZSM-5, is done by repeated ion exchange with a 1 *M* solution of ammonium nitrate, followed by washing with water, and finally by calcining in air at 800 K. The ZSM-5 samples were characterized by X-ray diffraction (XRD) on a Philips spectrometer equipped with a PW010 generator and a PW1050 goniometer. Spectra were recorded using Cu$K\alpha$ ray excitation. Scanning electron micrographs (SEM) were taken using a JEOL Model 2553 microscope. From XRD and SEM analyses, it was established that the samples are highly cristalline spherical agglomerates of ZSM-5 crystallites. Sizes of the agglomerates vary between 1 and 5 μm. Elemental analysis was performed by proton-induced X- and γ-ray emission (PIXGE) using a 4-MeV energy proton beam (*21*) from a Van de Graaff accelerator. A ZSM-5 batch, with a Si/Al atomic ratio of 35, and designated as Z1, was used for the preparation of most of the iron-supported catalysts. A second batch, designated as Z2, was synthesized without aluminum in the reactant mixture and has a Si/Al atomic ratio of 400. PIXGE analysis showed that the Na contents in the active form, H-ZSM-5, are less than its limit of detection, 0.01 wt% Na. Traces of Zr and Fe were detected at levels of 200 ppm or less.

Iron deposition. Ferrocene was purchased from Strems Chemical. Dibenzoylferrocene was synthesized from ferrocene in our laboratory. A weighed quantity of H-ZSM-5 is suspended in a solution of a known amount of metallocene in ether or chloroform for 30 min. The organic solvent is then evaporated to give a dry homogeneous mixture of metallocene with H-ZSM-5, which is finally calcined under static air in an oven, where the temperature is gradually increased from room temperature to 820 K. The resulting samples are designated as as-prepared catalysts. The influence of parameters such as Si/Al ratio and iron in metallocene/H-ZSM-5 initial weight ratio on the final loading and the distribution of iron in the catalyst were studied. Preparation conditions are summarized in Table 1. Samples prepared from ferrocene are designated as *X* Fe/H-Z1 or H-Z2 where *X* is the weight percentage of iron in the catalyst. The indication DBZ distinguishes samples prepared with dibenzoylferrocene.

Catalyst characterization. The weight percentage of iron in the final sample was measured by atomic absorption. The results are listed in Table 1.

Infrared analysis of adsorbed pyridine was performed to determine the level of substitution of protonic acid sites in ZSM-5 by iron cations. Spectra were obtained at the Pittsburgh Energy Technology Center

following a procedure described by Rhee *et al.* (*22*).

XRD analyses of Fe/ZSM-5 samples were carried out on the apparatus used for ZSM-5 characterization.

Dispersion and oxidation states of selected as-prepared samples were studied by X-ray photoelectron spectroscopy (XPS). Spectra were acquired on a VG ESCALAB Mark II electron spectrometer equipped with a hemispherical electron analyzer. Samples were mounted on indium foils and analyzed in the constant-pass energy mode (20 eV), using an incident beam of Al$K\alpha$ X rays. Pressure in the chamber during spectral acquisition was less than 10^{-6} Pa. Ionic sputtering was performed on selected samples using a 5-keV Ar^+ beam of 2.5 $\mu A/cm^2$ current density. Spectra were recorded after 20 min and after an additional 60 min of sputtering. All binding energies were corrected for charging by referencing the binding energy scale to Si 2*p* at 102.8 eV.

Catalytic evaluation. Catalytic runs were carried out in a microcatalytic fixed bed reactor, made of 38-cm-long SS tube with a 6-mm inside diameter, where 1 g of catalyst is placed between two plugs of glass wool. Liquid reactants can be fed into the reactor using a HPLC Gilson pump. At the reactor exist, condensed fractions can be collected at 180, 0, and −80°C. Noncondensed products are sampled at selected times with a 16-loop Valco valve controlled by a timer.

Fischer–Tropsch runs are performed with a CO/H_2 = 49.8/50.2 mixture provided by Linde. Other gases employed are research grade helium, hydrogen and carbon monoxide from Linde, and 99.99% pure methanol was from Fisher.

Liquid and gas fractions are analyzed by gas chromatography on a Perkin–Elmer Sigma 115 apparatus equipped with two 6-ft × ⅛-in. Porapak Q columns.

A first series of methanol conversion tests (MTG Tests) was performed by feeding methanol at WHSV = 1.7 h^{-1} in a helium gas stream at a flow rate of 30 ml(STP)/min at atmospheric pressure. The reactor temperature was 673 K. After 2 h, the methanol feed was stopped and the products were allowed to desorb from the catalyst for an additional 2 h.

TABLE 1

Conditions for the Preparation of Supported Iron Catalysts (Calcination Time: 5 h)

Catalyst designation	Fe/solvent volume (g/ml)	Fe/ZSM5 in solution (g/g) × 100	wt% Fe supported
0.9 Fe/H-Z1	0.1	1	0.88
1.6 Fe/H-Z1	0.2	2	1.65
2.6 Fe/H-Z1	0.3	3	2.61
3.3 Fe/H-Z1	0.4	4	3.31
3.4 Fe/H-Z1	0.5	5	3.43
3.1 Fe/H-Z1	2.0	5	3.08
4.3 Fe/H-Z1	1.0	15	4.30
4.2 Fe/H-Z1	0.75	15	4.20
4.6 Fe/H-Z1	3.0	60	4.58
4.7 Fe/H-Z1	2.0	100	4.72
5.1 Fe/H-Z1	0.5	25	5.07
3.3 Fe/Na-TPA-Z1	0.5	25	3.32
5.0 Fe/H-Z1	1.25	25	5.03
1.8 Fe/H-Z1	0.25	2.5	1.80
0.5 Fe/H-Z2	0.1	1.0	0.50
1.4 Fe/H-Z2	1.5	15	1.41
2.2 Fe/H-Z2	1.25	25	2.16
1.0 Fe/H-Z2	3.0	60	1.00
0.6 Fe/H-Z2	2.0	100	0.63
2.0 Fe DBZ/H-Z1	0.5	2	1.98
5.6 Fe DBZ/H-Z1	0.5	6	5.65
7.1 Fe DBZ/H-Z1	0.5	8	7.15
8.6 Fe DBZ/H-Z1	0.5	10	8.57
15.8 Fe DBZ/H-Z1	0.5	20	15.8
4.6 Fe DBZ/H-Z1	0.5	5	4.62

A second series of tests (MeOH + CO tests) was run under similar conditions, except that the helium was replaced by CO and the pressure of the system was maintained at 2 × 10^6 Pa (300 psia). Catalysts were pretreated in a CO stream of 30 ml (STP)/min at 573 K for 15 h and then at 673 K for 2 h before injecting methanol.

Finally, tests for conversion (F–T tests) of synthesis gas ($CO/H_2 \simeq 1/1$) were run at a pressure of 2 × 10^6 Pa (300 psia), 1500 h^{-1} GHSV, and temperatures between 573 and 673 K. Each test was carried out for 24 h.

More detailed descriptions of the catalytic tests, catalyst pretreatment, and the product analysis procedure may be found in Ref. (*23*).

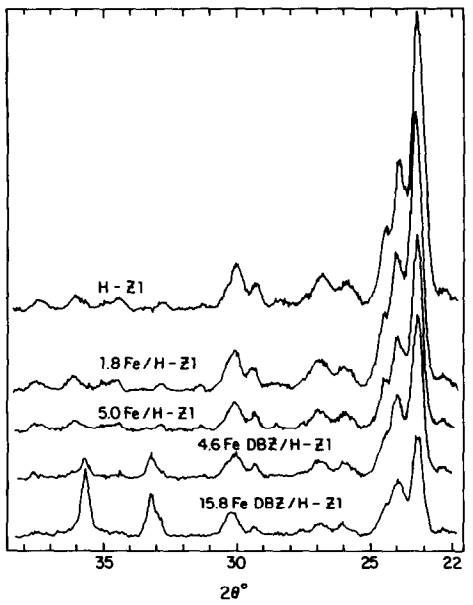

FIG. 1. X-Ray diffraction spectra of Fe/ZSM-5 catalysts and of the ZSM-5 support.

RESULTS AND DISCUSSION

Iron Loading of the Fe/ZSM-5 Catalysts

The variation of the final iron loading in each sample prepared from ferrocene, as a function of the total weight of iron introduced as ferrocene in solution per unit mass of ZSM-5 is reported in Table 1. Two ZSM-5 samples with different Si/Al ratios have been used as supports. These data show that the amount of iron which can be deposited by this method on ZSM-5 is limited to a maximum value. This is directly related to the volatilazation of ferrocene which occurs at a lower temperature (520 K) than its decomposition (740 K) (*19*). The quantity of iron fixed after calcination depends on the acidity of the support and on the rate of thermal decomposition of ferrocene compared to the rate of its volatilization.

The limitation in the amount of iron which can be fixed does not seem to exist when dibenzoylferrocene is employed instead of ferrocene. In this case, most of the iron present in the dry mixture is decomposed and fixed as iron oxide in the sample after calcination (see Table 1). This is definitely related to the absence of volatility of dibenzoylferrocene.

XRD Analysis

XRD spectra for the samples 1.8 Fe/H-Z1, 5.0 Fe/H-Z1, 4.6 DBZ Fe/H-Z1, 15.8 Fe DBZ/H-Z1, and H-Z1 are reproduced in Fig. 1. Spectra from samples prepared with ferrocene do not show any additional bands compared to the spectrum of the support. This indicates that iron is present in these samples as particles with sizes smaller than 50 Å. By contrast, intense bands of the iron oxide α-Fe_2O_3 (2θ = 33.1°, 35.6°) are exhibited by samples prepared from dibenzoylferrocene. This shows a poor dispersion of the iron in these catalysts.

Pyridine Adsorption Results

Figure 2 shows the IR spectra of pyridine chemisorbed on the samples 1.8 Fe/H-Z1 (curve a) and H-Z1 (curve b). Curve a is typical of the spectra obtained with Fe/ZSM-5 samples and curve b is typical of H-ZSM-5. After pyridine adsorption, three bands appear between wavenumbers 1600 and 1400 cm^{-1}. The band at 1545 cm^{-1} is

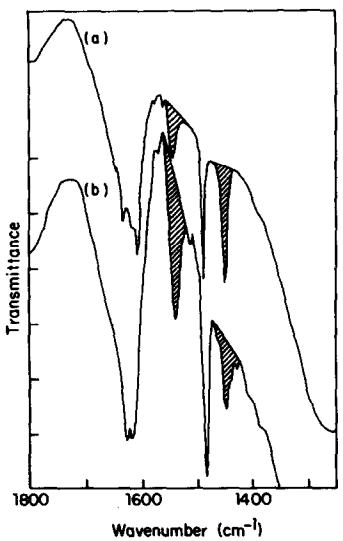

FIG. 2. Infrared spectra of chemisorbed pyridine. (a) 1.8 Fe/H-Z1, (b) H-Z1.

TABLE 2

Results from IR Spectra of Adsorbed Pyridine

Sample designation	$\nu_{Brønsted}$ (cm^{-1})	ν_{Lewis} (cm^{-1})	ν_{OH} (cm^{-1})	A_B/A_L[a]	Fe^{2+}/u.c.[b]	B/u.c.	wt% Fe exchanged
H-Z1	1544	1452	3730	1.46	—	1.39	—
1.8 Fe/H-Z1	1546	1452	3726	0.38	0.33	0.74	0.32
5.0 Fe/H-Z1	1544	1454	3727	0.10	0.56	0.27	0.54
4.6 Fe DBZ/H-Z1	1559	1440	3730	0.43	0.30	0.79	0.29

[a] Ratio of absorbances at $\nu_{Brønsted}$ (A_B) and ν_{Lewis} (A_L).
[b] u.c. = unit cell of H-Z1 (Si/Al = 35).

attributed to pyridium ions and is consequently associated with Brønsted acid sites (B). The band at 1450 cm^{-1} is assigned to pyridine molecules coordinatively bonded to Lewis acid sites (L). Two types of sites contribute to Lewis acidity; those associated with the aluminum atoms of the zeolite and formed by dehydroxylation of Brønsted acid sites at temperatures higher than 400°C (*25*), and those associated with counterions like Fe^{2+} inside the zeolite. A third band, appearing near wavenumber 1480 cm^{-1}, is common to pyridine adsorbed on both types of acid sites. In the OH band region, the catalysts Fe/ZSM-5 as well as the support show two IR bands. One at 3600 cm^{-1} is characteristic of Brønsted acid groups and it disappears upon pyridine adsorption due to the formation of pyridinium ions. Another band at 3730 cm^{-1} belongs to weakly acid silanol groups and does not interact with pyridine. The frequencies of the OH, Lewis, and Brønsted bands and the associated intensities ratio A_B/A_L observed for some samples are listed in Table 2. The A_B/A_L ratios measured for Fe/ZSM-5 samples are much lower than the value measured on the ZSM-5 support. This indicates a decrease in the Brønsted acidity upon iron deposition due to ion exchange of protons with iron cations. As shown by XPS results discussed later, the exchanged iron seems to be in a +2 oxidation state. The degree of ion exchange has been evaluated quantitatively with a method proposed by Stencel *et al.* (*26*) for Co/ZSM-5 catalysts.

The absorbance A of an IR absorption band is related to the concentration of the species responsible for the vibration following the Beer–Lambert law

$$A_\nu = C \times l \times \varepsilon_\nu,$$

where C is the concentration of adsorbate (μmole/cm^3), l is the thickness of the sample (cm), and ε_ν is the extinction coefficient at wavenumber ν. This relation leads to the ratio

$$B/L = (A_B/A_L) \cdot (\varepsilon_L/\varepsilon_B),$$

where B and L are, respectively, the concentrations of pyridine adsorbed on Brønsted and Lewis acid sites in the sample. As suggested by Stencel *et al.* (*26*), we have chosen the value of 1.5 for ε_B/e_L. All calculations are reported to a unit cell of ZSM-5. As Stencel *et al.* have shown that the most probable number of pyridine molecules adsorbed on a Co^{2+} cation is 2, we assumed the same value for Fe^{2+}. The number of Lewis acid sites due to dehydroxylation of the zeolite is calculated from the IR spectrum of the support, H-Z1. We assumed that no further dehydroxylation occurs as the calcination of the iron-supported samples was carried out at the same temperature as for the activation of Z1. Following the calculation steps of Ref. (*26*), the final results are shown in Table 2. The extent of the dehydroxylation of the ZSM-5 support is important, as indicated by the number of Brønsted acid sites after activation, 1.4/unit cell. The theoretical value is 2.7 proton/unit cell for ZSM-5 with Si/Al = 35. In addition, the original number

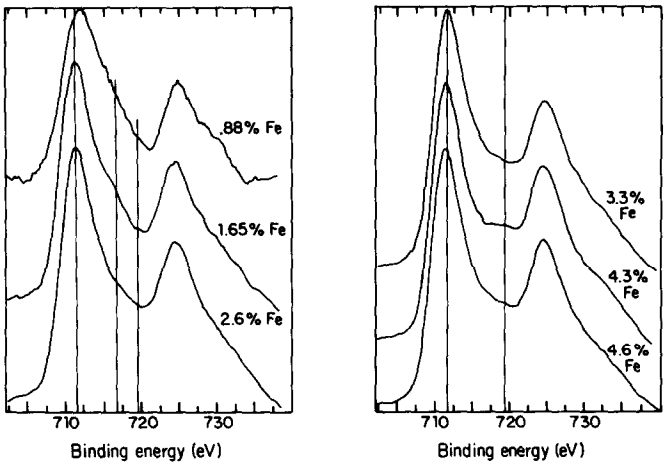

FIG. 3. ESCA spectra (Fe_{2p} lines) of Fe/ZSM-5 catalysts prepared with ferrocene.

of Brønsted acid sites in ZSM-5 drops to a four to five times lower value due to ion exchange with Fe^{2+} in the 5.0 Fe/H-Z1 sample. The degree of ion exchange increases with the iron content for the catalysts prepared with ferrocene. Meanwhile, the use of dibenzoylferrocene for iron deposition results in a less important ion exchange for comparable iron loadings (compare the samples 4.6 Fe DBZ/H-Z1 and 5.0 Fe/H-Z1). Hence, although deposition of iron using the bulky ferrocene derivative does not eliminate ion exchange, this phenomenon is at least limited in comparison with ferrocene-deposited samples. Nevertheless, iron involved in ion exchange with protons is only a very small portion of the total deposited iron in both cases, as shown by the values in the last column of Table 2.

Surface Characterization

XPS spectra of the Fe 2*p* region for a series of as-prepared catalysts produced with ferrocene are shown in Fig. 3. At low iron loading, the presence of a satellite at +6.0 eV in the Fe $2p_{3/2}$ line would be characteristic of Fe^{2+}. However, the binding energy of the Fe $2p_{3/2}$ band, 711.8 eV for sample 0.9 Fe/H-Z1, is much higher than the value of 709.7 ± 0.2 eV expected for Fe(II) according to the literature data (*27, 28*). This higher value is ascribed to the highly ionic character of the Fe^{2+} counterion associated with ZSM-5. As the iron content increases, the Fe 2*p* band shape characteristic of oxidation state 3+, with a weak satellite peak at about 719 eV, becomes prevalent. This is ascribed to the build up of Fe_2O_3 particles on the external surface ZSM-5 particles.

Figure 4 shows variations of $(Fe/Si)_{XPS}$ atomic ratio, calculated from the peak area of Si 2*p* and Fe 2*p* bands, as a function of the bulk atomic ratio $(Fe/Si)_b$. The XPS peak intensity I_i is related to the concentration n_i of an element i by

$$I_i = F \cdot S \cdot \sigma_i \cdot D_i \cdot n_i \cdot \lambda_i$$

where S is the area of the surface analyzed, F is the X-ray flux, D_i is the detection efficiency of the spectrometer, σ_i is the cross section of the emission, and λ_i is the escape depth. It is convenient to calculate a nominal ratio of atomic concentrations in the first layers of the sample sensed by ESCA:

$$\left(\frac{Fe}{Si}\right)_{XPS} = \frac{n_{Fe}}{n_{Si}} = \frac{I_{Fe}}{I_{Si}} \cdot \frac{\sigma_{Si}}{\sigma_{Fe}} \cdot \frac{\lambda_{Si}}{\lambda_{Fe}} \cdot \frac{D_{Si}}{D_{Fe}}.$$

For the VG ESCALAB II, the detection efficiency is proportional to $(E_k)^{-1/2}$ where E_k is the kinetic energy of the emitted electron. Cross sections are given by Scofield (*29*). Escape depths are average values (λ_{Fe} = 1.5 nm, λ_{Si} = 2.44 nm) calculated from empirical formulas which relate λ to E_k, as

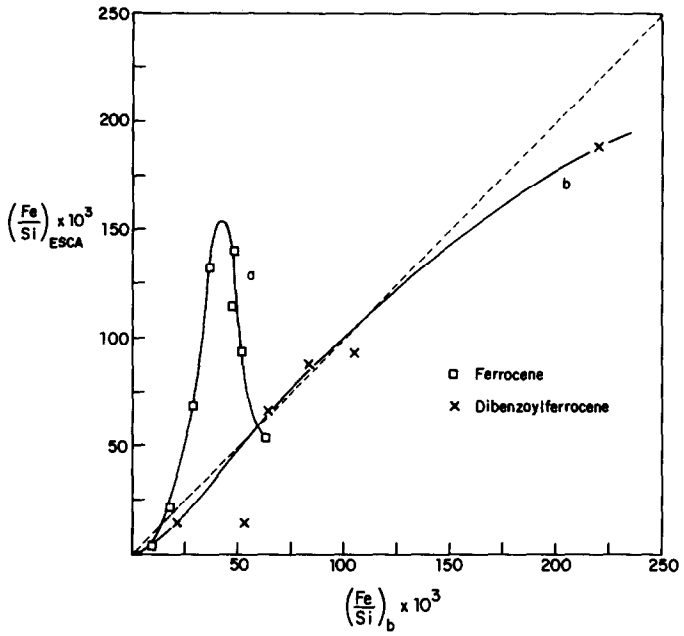

FIG. 4. $(Fe/Si)_{XPS}$ atomic ratio calculated from ESCA intensity ratio as a function of bulk atomic ratio $(Fe/Si)_b$ for Fe/ZSM-5 catalysts prepared with ferrocene (a) and dibenzoylferrocene (b).

given by Vulli and Starke (*30*), Chang (*31*), and Penn (*32*). For samples prepared with ferrocene, the $(Fe/Si)_{XPS}$ ratio increases dramatically with bulk ratio at low loadings, to reach a maximum for an iron concentration of about 4 wt%. These high values of $(Fe/Si)_{XPS}$, compared to corresponding $(Fe/Si)_b$, denote a high segregation of the iron in the first layers of these Fe/ZSM-5 catalysts. At loadings higher than 4%, $(Fe/Si)_{XPS}$ decreases rapidly.

XRD analyses indicate the absence of iron oxide with particle sizes greater than 50 Å. This suggests a high dispersion of iron, possibly as a monolayer on the external surface of ZSM-5. We have not measured the external surface area of our ZSM-5 samples, but Namba and Yashima (*33*) found a value of 25 m^2/g for ZSM-5 particles of the same size and morphology. In addition, the average cross section of a unit cell of Fe_2O_3 can be estimated to be 30 $Å^2$ according to its spinel structure. Hence, the monolayer saturation of the external surface of ZSM-5 particles with Fe_2O_3 oxide would correspond roughly to 1.7 wt% iron. This value can be compared to the iron percentage equivalent to a monolayer dispersion on the external surface of ZSM-5 calculated from XPS intensity ratio (I_{Fe}/I_{Si}) by assuming that the contribution to the iron signal from iron fixed inside the support in negligible. A simple model, developed for this purpose, is reported in (*23*) and the corresponding results are listed in Table 3. Iron loadings calculated for samples 3.3 Fe/H-Z1 and 4.3 Fe/H-Z1, corresponding to the maximum ratio $(Fe/Si)_{XPS}$, as shown in Fig. 4, are lower than the theoretical maximum iron loading of 1.7% for a monolayer of Fe_2O_3. These results give a certain plausibility to the monolayer model. In other words, iron deposited on the external surface of ZSM-5 is highly dispersed in the samples corresponding to the ascending part of the curve a in Fig. 4. Interestingly, these samples also correspond to an initial ascending part of the curve relating the weight percentage of deposited iron as a function of total iron introduced as ferrocene (Table 1).

The descending branch of curve a in Fig.

TABLE 3

Hypothetical Percentage Fe Values Corresponding to a Monolayer Coverage of the External Surface of ZSM-5 Particles and Yielding the Experimental Value for ($I_{Fe\,2p}/I_{Si\,2p}$)

Sample designation	I_{Fe}/I_{Si}	(wt% Fe)$_{mono}$	Surface coverage %	Fe_{mono} %/Fe_{total}
0.9 Fe/H-Z1	0.074	0.035	2.1	3.9
1.6 Fe/H-Z1	0.43	0.20	11.8	12.0
1.8 Fe/H-Z1	0.26	0.12	7.1	6.7
2.6 Fe/H-Z1	1.38	0.60	35.3	25.1
3.3 Fe/H-Z1	2.67	1.30	76.5	38.1
4.3 Fe/H-Z1	2.80	1.35	79.4	31.5
4.6 Fe/H-Z1	1.9	0.90	53	19.5
5.0 Fe/H-Z1	1.03	0.48	28.2	9.6

4 could have two explanations. Either the external segregation would decrease, or the dispersion of the externally segregated iron decreases with loading. However, in the second eventuality, the iron oxide particles should remain smaller than 50 Å, as indicated by XRD results. In order to check for this second hypothesis, a calculation was made for the sample 5.0 Fe/H-Z1 with the highest loading. Assuming that iron oxides deposited on the external surface of the support as cubic particles of 50-Å edge size, a weight percentage for iron has been calculated from the experimental ($I_{Fe\,2p}/I_{Si\,2p}$) ESCA intensity ratio (*23*). This model yields a value of 1.7 wt% Fe.

Assuming that the ESCA signal after sputtering is representative of iron loading inside the zeolite matrix, a value of 3 wt% Fe is calculated from the corresponding value of $(Fe/Si)_{XPS}$. Therefore, the total calculated loading of this sample would be 4.7%, a value close to the 5% iron content in this sample.

In summary, up to 4% iron loading, deposition from ferrocene results in a highly dispersed iron oxide on the external surface of ZSM-5 particles. When a maximum amount of 5% iron is reached, partial agglomeration occurs, the oxide still being in a good dispersion state.

Similar analyses have been carried out on samples prepared with dibenzoylferrocene. Spectra of the Fe_{2p} bands for all samples display band shapes characteristic of Fe^{3+} species, even at the lowest iron loading of 2.0 wt%. The $Fe_{2p\,3/2}$ binding energy is close to 710 eV, which is about 1 eV lower than the expected value of Fe^{3+} in Fe_2O_3. Such a difference could result from an overestimation of the binding energy correction due to charging and may happen if the iron particles are poorly dispersed on the support instead of being in intimate contact with ZSM-5. Curve b of Fig. 4 shows that iron dispersion in the sample is not strongly affected by iron loading, as $(Fe/Si)_{XPS}$ steadily increases with $(Fe/Si)_b$. This observation and the XRD results lead to the conclusion that a sample prepared from dibenzoylferrocene is a homogeneous mixture of large Fe_2O_3 particles with ZSM-5 particles.

Catalytic Tests

MTG tests. For MTG tests run under the conditions previously described with catalysts 1.8 Fe/H-Z1, 5.0 Fe/H-Z1, 4.6 Fe DBZ/H-Z1, and H-Z1, the distributions of the products obtained are given in Table 4. Full conversion is reached in all cases. It is interesting to note that the addition of iron induces a higher C_5^+ fraction in hydrocar-

TABLE 4

Results of MTG Tests[a]

	Catalyst designation			
	H-Z1	1.8 Fe/H-Z1	5.0 Fe/H-Z1	4.6 Fe DBZ/H-Z1
Product distribution, wt%				
$CO + H_2$	1.1	2.5	0.7	0.7
H_2O	55.6	54.5	54.9	53.5
Hydrocarbons	43.4	43.0	44.4	45.8
Hydrocarbon distribution, wt%				
CH_4	0.8	0.9	0.9	0.6
C_2–C_4	51.9	41.6	41.9	42.0
% Olefins in (C_2–C_4)	5.8	17.8	32.0	18.6
C_5^+	47.3	57.5	57.2	57.4
% Aromatics in C_5^+	65.9	46.4	45.2	46.3

[a] Conditions: temperature 400°C; pressure ≈ 1 atm; $WHSV_{CH_3OH}$, 1.7 h^{-1}; helium flow rate 30 ml(STP)/min.

bons and a lower aromatic content in C_5^+ fraction. This is linked to a partial loss of Brønsted acid sites of the ZSM-5 support upon iron deposition, a result in agreement with those of pyridine chemisorption measurements. This affects mainly the last steps in the MTG reaction mechanism such as secondary cracking of C_5^+, aromatic synthesis and alkylation with olefins, and hydrogen transfer from naphthenics to olefins. This tendency increases with iron loading for catalysts prepared with ferrocene, as shown by the comparison of product distributions found over 1.8 Fe/H-Z1 and 5.0 Fe/H-Z1. It is also noteworthy that even a fourfold decrease in Brønsted acid sites in the second sample still allows a full conversion of methanol to hydrocarbons. Moreover, the 4.6 Fe DBZ/H-Z1 catalyst seems to be less affected by iron deposition than the one prepared using ferrocene with similar iron loading. This catalyst gives a hydrocarbon product distribution very close to the distribution obtained on 1.8 Fe/H-Z1 whereas both samples possess almost the same concentration of protonic sites, as shown in Table 2.

Fischer–Tropsch tests. Conversion and product distributions for a few F–T tests are reported in Table 5 along with results from the literature for Fe/ZSM-5 catalysts at 300°C. The tests performed on 3.0 Fe/H-Z1 show that conversions of CO and H_2 increase with temperature along with the importance of WGS as shown by the increasing CO_2 and decreasing H_2O content in the products. No hydrocarbon heavier than C_{10} was observed in the products, as expected from the shape selective properties of ZSM-5. Chang *et al.* (*34*) suggest that competition exists between hydrogenation over the metal function of the olefins produced as primary products in the F–T synthesis, followed by desorption of the saturated compounds, and conversion of these olefins into C_5^+ and aromatic hydrocarbons on the acid sites of the ZSM-5. As shown by the hydrocarbon distribution, an increase in temperature favors the hydrogenation as CH_4 production increases and the formation of C_5^+ hydrocarbons dramatically decreases.

Comparison of the results obtained on 3.0 Fe/H-Z1 and 5.0 Fe/H-Z1 at 400°C indicates that higher iron loading induces higher conversion of synthesis gas while

TABLE 5

Results of Fischer–Tropsch Tests ($H_2/CO \simeq 1$)

	Catalyst designation					
	5.8% Fe/ZSM-5 from Ref. (*13*)	16% Fe/ZSM-5 from Ref. (*35*)	3.1 Fe/H-Z1	3.1 Fe/H-Z1	3.1 Fe/H-Z1	5.0 Fe/H-Z1
Temperature (°C)	300	300	300	350	400	400
Pressure (psi)	200	300	300	300	300	300
GHSV (h^{-1})	1600	1000	1500	1500	1450	1200
Pretreatment	—	—	—[a]	Run at 300°C	Run at 350°C	—[a]
CO conversion %	51.5	54	7.5	27.0	48.0	61
H_2 conversion %	57.1	62	15.0	38.0	55.5	58
CO + H_2 conversion %	—	—	11.3	32.5	51.8	59.5
Product distribution, wt%						
CO_2	51.2	52.0	24.3	52.7	63.6	66.5
H_2O	19.0	17.3	33.3	14.3	6.0	5.3
Hydrocarbons	29.8	30.7	42.4	33.0	30.4	28.2
Hydrocarbon distribution, wt%						
CH_4	23	37	58.0	68.5	74.0	41.5
C_2–C_4	23	28	21.0	27.1	24.4	38.6
C_5^+	54	35	21.0	4.4	1.6	19.9
% Aromatics in C_5^+	14	9	66	59	39	42

[a] Reduction H_2, 500°C, 30–60 psia, 30–50 ml (STP)/min, 15 h.

the WGS reaction is barely affected. The most striking effect related to the increase in the iron content is the much lower selectivity for CH_4 production, accompanied by a higher production of C_2–C_4 and C_5^+. Table 5 includes results reported in the literature for similar Fe/H-ZSM-5 catalysts under comparable operating conditions. Stencel *et al.* (*35*) found a selectivity of 37% toward CH_4 production on a 15% Fe/H-ZSM-5 catalyst, where the metal is present as 60-Å iron particles. Butter *et al.* (*13*) observed a CH_4 selectivity of 23% on a 5.8% Fe/H-ZSM-5 prepared by impregnation with iron nitrate solution, a method which usually leads to a low metal dispersion. These results, together with the CH_4 selectivity of 58% obtained on our 3.0 Fe/H-Z1 sample, where according to XPS analysis iron is highly dispersed, suggest that small iron particles yield higher methane production. The same effect of iron particle size is observed on 5.0 Fe/H-Z1 which possesses less dispersed iron than 3.0 Fe/H-Z1, according to XPS characterization.

The variations with time-on-stream in the production rates of light reaction products collected in the 16-loop valve during the F–T test show that these catalysts have very stable activity in F–T conversion. This is related to the stability of the dispersion of iron in these samples at high temperature. Such steady activity also has been observed by Obermyer *et al.* (*36*) on a Fe/H-ZSM-5 catalyst with 60-Å iron particle size. Interaction between these small agglomerates and the acidic support may have a stabilizing effect on their size and the electronic state of iron atoms. In this context, Pommier *et al.* (*37*) recently proposed that iron oxides exhibit greater and more stable activity than metallic iron in the conversion of synthesis gas. They mention the absence of carbide formation on iron oxide-supported catalysts whereas metallic iron has a great tendency to form carbonaceous material in the presence of CO which causes rapid deactivation. It is possible that highly dispersed iron in a zeolitic matrix remains in a partially oxidated state after the pretreatment in H_2 and in the presence of the reducing reactant mixture during the reaction, and as a consequence it possesses a higher resistance to carbide formation.

MeOH + CO tests. Some results for MeOH + CO tests run on the same catalysts as the MTG tests are reported in Table 6. The conversion of methanol is complete, although a nonnegligible fraction of methanol is decomposed into CO and H_2 in the presence of iron. The reported % WGS value corresponds to the fraction of total water produced by methanol dehydration, converted to CO_2 and H_2 in the presence of CO

The most active catalyst for WGS is the one prepared from ferrocene with the highest iron loading, 5.0 Fe/H-Z1. Again, samples 4.6 Fe DBZ/H-Z1 and 1.8 Fe/H-Z1 have similar activities for the WGS activity. Moreover, a direct correlation between Fe^{2+} concentration and WGS activity seems to exist. This correlation may correspond to the fact that the active form of iron oxide for the WGS reaction is magnetite, Fe_3O_4, which contains Fe^{2+} ions. Even though more data are needed to confirm such a role for Fe^{2+}, it is tempting

TABLE 6

Results of MeOH + CO Tests[a]

	Catalyst designation			
	H-Z1	1.8 Fe/H-Z1	5.0 Fe/H-Z1	4.6 Fe DBZ/H-Z1
Product distribution, wt%				
$(CO + H_2)_{calcd}$	1.1	11.3	15.6	15.7
H_2O	53.4	33.4	17.8	29.8
% WGS	3.4	31.4	61.2	34.5
Hydrocarbons	43.6	40.0	38.5	38.8
Hydrocarbon distribution, wt%				
CH_4	1.7	3.5	10.1	5.1
C_2–C_4	46.7	37.3	39.3	39.5
% Olefins in C_2–C_4	1.3	4.8	4.6	4.8
C_5^+	51.6	59.2	50.6	55.4
% Aromatics in C_5^+	79.6	52.4	47.7	56.2

[a] Conditions: temperature 400°C; pressure 300 psia; $WHSV_{CH_3OH}$, 1.7 h^{-1}; CO flow rate, 30 ml(STP)/min. Pretreatment: CO, 300°C, 300 psi, 15 h + CO, 400°C, 300 psi, 2 h.

to ascribe the WGS activity in our catalysts to the Fe^{2+} ion stabilized in the zeolite pores, as suggested by the ESCA results.

The hydrogen produced by WGS and reincorporated in the hydrocarbon constitutes a small portion of the total molecular hydrogen evolved, due to the relatively poor hydrogenation activity of iron.

According to hydrocarbon compositions, H_2 produced in the WGS reaction may be reincorporated by reacting with CO to form CH_4 and by hydrogenation of small olefins. The increase of the olefin content in the C_2–C_4 fraction with respect to the product distribution observed on H-Z1 alone, due to ion exchange with Fe^{2+}, is less important than in the MTG test (see Table 4). This results from the interception of olefins by H_2 produced in the WGS reaction and to a lesser extent in methanol decomposition.

The rate of production of light compounds with time-on-stream shows that over 5.0 Fe/H-Z1, yields of CO_2 and light hydrocarbons are stable during the 2 h on stream. The same observation was made over 1.8 Fe/H-Z1, although in this case the WGS activity is lower than with 5.0 Fe/H-Z1. With sample 4.6 Fe DBZ/H-Z1 prepared with dibenzoylferrocene the rate of CO_2 production reaches a maximum, and then steadily decreases, indicating a loss in WGS activity with time. As in this sample the external iron oxide particles are much bigger than those in catalysts prepared with ferrocene, they may be less resistant to reduction. Therefore the decrease in activity observed with 4.6 Fe DBZ/H-Z1 could be associated with a transient decreasing concentration of Fe^{2+} species at the surface of the external iron oxide particles. Such a catalyst decay would not be obtained when the WGS activity is mostly associated with the Fe^{2+} ions present in the pores and stabilized by their interaction with the zeolite structure.

CONCLUSION

ZSM-5-supported iron catalysts prepared by calcination of ferrocene and dibenzoylferrocene display rather different structural and catalytic properties. XRD and XPS techniques both indicate that in the dibenzoylferrocene prepared samples iron is segregated at the outer surface of the ZSM-5 particles as a poorly dispersed Fe_2O_3 phase. Ferrocene prepared catalysts show a more uniform spatial distribution and a greater dispersion of iron oxide. XPS also shows that part of the iron is present in the pores as Fe^{2+} ions, a conclusion sustained by both results of IR adsorbed pyridine and MTG catalytic tests. The concentration of Fe^{2+} seems to be correlated with the WGS activity, as observed during MeOH + CO tests at 400°C. The highly dispersed iron oxide seems to favor methanation during F–T tests.

The F–T tests showed that at 400°C, Fe/ZSM-5 catalysts have a high WGS activity and retain some CO hydrogenation activity. However, MeOH + CO tests show that although much of the water produced by dehydration of methanol is effectively converted by WGS, the relative rate of CO hydrogenation is not sufficient to allow an important reincorporation of hydrogen in the hydrocarbon products over these Fe/ZSM-5 catalysts. This result suggests that for an effective deoxygenation by CO the successful catalysts will have to incorporate, in addition to iron, a third catalytic function favoring hydrogenation.

REFERENCES

1. Kaliaguine, S., "Upgrading Pyrolytic Oils from Wood and Other Biomasses," NSERC Project 036-1326 10274. Ottawa, Canada, 1981.
2. Overend, R., "Canada's Biomass Conversion Technology R & D Program," *in* Thermal Conversion of Solid Waste and Biomass, *ACS Symp. Ser.* **130,** 317 (1980).
3. Chang, C. D., and Silvestri, A. J., *J. Catal.* **47,** 249 (1977).
4. Stowe, R. A., and Murchison, C. B., *Hydrocarbon Process.* **1,** 147 (1982).
5. Haag, W. O., Rodewald, P. G., and Weisz, P. B., U.S. Pat. 4,300,009 (1981).
6. Weisz, P. B., Haag, W. O., and Rodewald, P. G., *Science* **206,** 57 (1979).
7. Prasad, Y. S., Bakshi, N. N., Eager, R. L., and

Mathews, J. F., *Stud. Surf. Sci. Catal.* **19,** 85 (1984).
8. Frankiewicz, T. C., U.S. Pat. 4,308,411 (1981).
9. Mathews, J. F., Tepylo, M. G., Eager, R. L., and Pepper, J. M., *Can. J. Chem. Eng.* **63,** 686 (1985).
10. Chantal, P., Kaliaguine, S., Grandmaison, J. L., and Mahay, A., *Appl. Catal.* **10,** 317 (1984).
11. Newsome, D. S., *Catal. Rev. Sci. Eng.* **21,** 275 (1980).
12. Caesar, P. D., Brennan, J. A., and Garwood, W. E., *J. Catal.* **65,** 328 (1980).
13. Butter, S. A., Chester, A. W., and Schwartz, A. B., U.S. Pat. 4,298,695 (1981).
14. Melson, G., Crawford, J. A., Crites, J. W., Mbadcam, K., Stencel, J., and Rao, V. U. S., *ACS Symp. Ser.* **218,** 397 (1983).
15. Rao, V. U. S., Gormley, R. J., Schehl, R. R., Rhee, K. N., Chi, R. D. H., and Pantages, G., *in* "Proc., Symp. Conv. Synth. Gas Alcohols Chem. 1983," p. 151. Plenum, New York, 1984.
16. Hyang, J. J., and Haag, W. O., *ACS Symp. Ser.* **152,** 307 (1981).
17. Ballivet-Tkatchenko, D., Chau, N. D., Mozzanega, H., Roux, M. C., and Tkatchenko, I., *ACS Symp. Ser.* **152,** 187 (1981).
18. Bein, T., and Jacobs, P. A., *J. Chem. Soc. Faraday Trans 1* **79,** 1819 (1983).
19. Rosenblum, M., "Chemistry of the Iron Group Metallocene. Part I." Wiley, New York, 1965.
20. Gabelica, Z., Derouane, E. G., and Blom, N., *Appl. Catal.* **5,** 227 (1983).
21. Szöghy, I. M., Mahay, A., and Kaliaguine, S., *Zeolites* **6,** 39 (1986).
22. Rhee, K. H., Rao, V. U. S., Stencel, J. M., Melson, G. A., and Crawford, J. E., *Zeolites* **3,** 337 (1983).
23. Mahay, A., Ph.D. thesis. Université Laval, 1986.
24. Parker, L. M., Bibby, D. M., and Patterson, J. E, *Zeolites* **4,** 168 (1984).
25. Vedrine, J. C., Auroux, A., Bolis, V., Dejaivfe, B., Naccache, C., Wierzchowski, P., Derouane, E. G., Nagy, J. B., Gilson, J. P., van Hoof, J. H. C., Van den Berg, J. P., and Wolthuizen, J., *J. Catal.* **59,** 248 (1979).
26. Stencel, J. M., Rao, V. U. S., Diehl, J. R., Rhee, K. H., Dhere, A. G., and DeAngelis, R. J., *J. Catal.* **84,** 109 (1983).
27. Brundle, C. R., Chuang, T. J., and Wandelt, K., *Surf. Sci.* **68,** 459 (1977).
28. McIntyre, N. S., and Zetaruk, D. G., *Anal. Chem.* **49,** 1521 (1977).
29. Scofield, J. H., *J. Electron Spectrosc. Relat. Phenom.* **8,** 129 (1976).
30. Vulli, M., and Starke, K., *J. Phys. E* **10,** 158 (1978).
31. Chang, C. C., *Surf. Sci.* **48,** 9 (1975).
32. Penn, D. R., *J. Electron Spectrosc. Relat. Phenom.* **9,** 29 (1976).
33. Namba, S., and Yashima, T., *J. Catal.* **81,** 485 (1983).
34. Chang, C. D., Lang, W. H., and Silvestri, A., *J. Catal.* **56,** 268 (1979).
35. Stencel, J. M., Diehl, J. R., Douglas, L. J., Spitler, C. A., Crawford, J. E., and Melson, G. A., *Colloids Surf.* **4,** 331 (1982).
36. Obermyer, R. T., Mulay, L. N., Lo, C., Oskooie-Tabrizi, M., and Rao, V. U. S., *J. Appl. Phys.* **53,** 2683 (1982).
37. Pommier, B., Reymond, J. P., and Teichner, S. J., *Stud. Surf. Sci. Catal.* **19,** 436 (1984).

A. MAHAY
G. LEMAY
A. ADNOT
I. M. SZÖGHY
S. KALIAGUINE

Department of Chemical Engineering
Department of Physics and GRAPS
Université Laval, Québec, Canada

Received June 10, 1986